Journal of Molecular Graphics and Modelling 79 (2018) 157–165

Contents lists available at ScienceDirect

Journal of Molecular Graphics and Modelling

journal homepage: www.elsevier.com/locate/JMGM

Reaction profiling of a set of acrylamide-based human tissue transglutaminase inhibitors

Mahmood H. Jasim [1], Daniel L. Rathbone *

School of Life and Health Sciences, Aston University, Birmingham B4 7ET, United Kingdom

ARTICLE INFO

Article history:
Received 11 July 2017
Received in revised form 13 October 2017
Accepted 16 October 2017
Available online 22 November 2017

Keywords:
Tissue transglutaminase
Irreversible inhibitors
Molecular docking
Molecular dynamics
Umbrella sampling

ABSTRACT

The major function of the enzyme human tissue transglutaminase (TG2) is the crosslinking of proteins via a transamidation between the γ-carboxamide of a glutamine and the ε-amino group of a lysine. Overexpression of TG2 can lead to undesirable outcomes and has been linked to conditions such as fibrosis, celiac disease and neurodegenerative diseases. Accordingly, TG2 is a tempting drug target. The most effective TG2 inhibitors to date are small-molecule peptidomimetics featuring electrophilic warheads that irreversibly modify the active site catalytic cysteine (CYS277). In an effort to facilitate the design of such TG2 inhibitors, we undertook a quantum mechanical reaction profiling of the Michael reaction between a set of six acrylamide-based known TG2 inhibitors and the TG2 CYS277. The inhibitors were docked into the active site and the coordinates were refined by MD simulations prior to modelling the covalent modification of the CYS277 thiolate. The results of QM/MM MD umbrella sampling applied to reaction coordinates driving the Michael reaction are presented for two approximations of the Michael reaction: a concerted reaction (simultaneous thiolate attack onto the acrylamide warhead and pronation from the adjacent HIS335) and a two-stage reaction (consecutive thiolate attack and protonation). The two-stage approximation of the Michael reaction gave the better results for the evaluation of acrylamide-based potential TG2 inhibitors *in silico*. Good correlations were observed between the experimental TG2 IC_{50} data and the calculated activation energies over the range 0.0061–6.3 μM (three orders of magnitude) and we propose that this approach may be used to evaluate acrylamide-based potential TG2 inhibitors.

1. Introduction

Human tissue transglutaminase, also known as transglutaminase 2 (TG2) is a member of the transglutaminase family of enzymes. A major function of TG2 is the crosslinking of proteins via a calcium-dependent transamidation between the γ-carboxamide of a glutamine and an ε-amino group of a lysine [1]. Physiologically, TG2 activity is associated with regulation of the extracellular matrix (ECM) formation, cell adhesion, wound healing, signal transduction, apoptosis, and stabilisation of skin and hair [1–3].

Overexpression of TG2, however, can lead to undesirable outcomes. For example, increased TG2 activity has been noted in neurodegenerative diseases such as Parkinson's, Alzheimer's and Huntington's [4–6] as well as in celiac disease [7]. Furthermore, the inhibition of TG2 activity has been shown to reduce metastasis in pancreatic and lung cancers [8,9]. Three of the major classes of TG inhibitors that have been exemplified include: competitive reversible inhibitors such as cystamine [10,11]; reversible non-competitive inhibitors that act by binding to an allosteric site within TG2 preventing its activation [12,13]; irreversible inhibitors containing an electrophilic warhead that act by alkylating the key active site cysteine. (References given below) In the biological setting, any inhibitor targeting the active site of TG2 has to overcome the locally high total concentration of potential substrates, for example competition with fibronectin vitronectin, osteonectin, osteopontin, laminin, fibrillin, nidogen, collagens I, II V and XI in the extracellular matrix [14]. For this reason, despite reservations over potential toxicity and off-target activity, irreversible inhibitors may, in the end, provide therapeutic inhibitors of this enzyme. Most of the irreversible inhibitors published to date are peptidic or peptidomimetic and contain an electrophilic group capable of reacting with a cysteine thiolate anion, for example, maleimides, epoxides, acrylamides, chloroacetamides, beta-keto sulfonium ions and substituted imadazolium groups [15–21].

Following on from a series of irreversible dipeptide-based inhibitors (Fig. 1**a**) featuring the beta-keto sulfonium warhead [16],

* Corresponding author.
E-mail address: D.L.Rathbone@aston.ac.uk (D.L. Rathbone).
[1] On secondment from the College of Pharmacy, University of Mosul, Mosul, Iraq and funded by the Iraqi Ministry of Higher Education and Scientific Research.

https://doi.org/10.1016/j.jmgm.2017.10.012

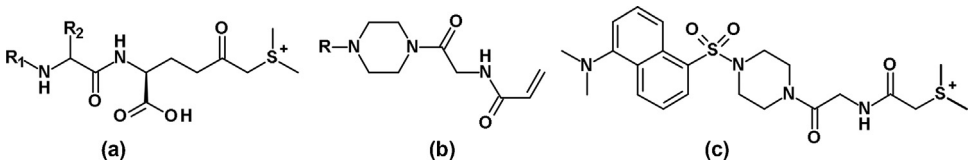

Fig. 1. Irreversible TG2 inhibitor types and a fluorescent example published by the Griffin group.

the Griffin group has published a set of conformationally-restricted inhibitors (Fig. 1**b**) featuring the piperazinyl-glycylacrylamide core structure [15,21].

The piperazine portion serves to constrain the flexibility of the central region of the compounds and the glycylacrylamide is able to reach into the active site tunnel to allow a Michael reaction to occur between the thiolate anion of CYS277 and the beta carbon of the acrylamide. The other piperazine nitrogen is bound to a series of hydrophobic entities via amide, carbamate and sulfonamide linkages. In support of the presumed site of reaction for the acrylamide compounds being CYS277, the Griffin group [15] has profiled a close analogue of acrylamide compound **5** (Table 1) featuring a beta-keto sulfonium warhead in place of the acrylamide (Fig. 1**(c)**). Recombinant wild-type TG2 and its active site mutant CYS277SER were incubated with the compound. Subsequently, TG2 was separated on denaturing SDSPAGE and western blotted using an anti-dansyl antibody. The observed bands indicated that the inhibitor had been covalently incorporated into the wild-type enzyme but not the CYS277SER mutant form.

Our initial attempts to use computer-based protein-ligand docking methods (data not presented) to search for irreversible inhibitors of TG2 were successful to the extent of distinguishing between moderate-high potency inhibitors and non-inhibitor analogues. It was not possible, however, to rank compounds according to potency at the good-high potency end. In retrospect this is not surprising, since in the case of irreversible covalent binding of the inhibitor to the active site, placement of the inhibitor in the active site is only one part of the overall process. For example, it is possible for a compound to fit very well into the active site but for the subtleties of its arrangement in the active site to impair its ability to derivatise the CYS277 thiolate anion. Therefore, as an attempt to develop a computational screening tool to allow the ranking of acrylamide-containing small molecules as irreversible TG2 inhibitors, we decided to implement a QM/MM umbrella sampling approach to investigate the covalent bond-forming stage. Thus the overall approach was to dock the potential inhibitors into the active site of a TG2 model, conduct MD upon the complexes, select plausible starting positions for an approximation to the thiolate-acrylamide Michael reaction and to probe the energy profile of the reaction coordinate via umbrella sampling.

2. Methods

MM-MD simulations were performed using a CUDA-ported version of Amber 12 [22–25] on workstations and servers equipped with Nvidia GTX 780, GTX 780 Ti or Titan graphics cards. QM MM-MD hybrid calculations [26,27] were performed using Amber 12 on an Intel Xeon-based server. The trajectories were processed using PTRAJ or CPPTRAJ [28]. The production phases of all MD trajectories were analysed with respect to temperature, pressure and RMSD and found to be stable.

2.1. The inhibitors

Six irreversible TG2 inhibitors featuring an acrylamide warhead were used in this work (Table 1). They were adopted from Badarau et al [15].

2.2. Preparation of TG2 active site models and complexes

Our models for the open form of TG2 were derived from a repaired version of the Protein Data Bank entry 2Q3Z [29] in which the missing residues were added and the existing covalently-bound inhibitor was deleted. CYS277 was set to its ionised form and HIS335 was allocated its protonated form following the generally accepted view that the catalytic triad CYS277, HIS335, ASP358 is arranged such that the cysteine and the histidine exist as a thiolate-imidazolium pair stabilised by hydrogen bonding to ASP358 [30,31]. In order to maximise the computational speed, the sandwich and barrel domains at the furthest extremes of the protein structure (residues 1–154 and 586–683) were deleted. During the course of an exploratory 250 ns MD simulation of the entire enzyme in explicit water, the amino acid residues within 8 Å of CYS277 were found to have an average RMSD of 0.82 Å using the first frame as a reference. Furthermore, the catalytic triad residues CYS277, HIS335, ASP358 exhibited individual RMSF values of 0.38, 0.31 and 0.36 Å respectively. The same procedure applied to the truncated enzyme resulted in an average RMSD of 0.92 Å and RMSF values for CYS277, HIS335 and ASP358 of 0.33, 0.30 and 0.35 Å respectively. This supported our view that the peripheral sandwich and barrel domains were too far away from the active site core region to have any effect upon the active site in the timescale of the simulations reported in this work. These regions are identified in yellow in Fig. S**1a** in the supplementary information.

The truncated version of the repaired enzyme was relaxed using a combination of energy minimisation and molecular dynamics (100 ns production phase) in explicit water using the Amber 12 package. Further details are given in the supplementary information. Models for the active site were taken from the resultant trajectory and probed by docking active TG2 irreversible inhibitors taken from the work of Badarau et al. [14] and Griffin et al. [16] using the programs CACHe WorkSystem Pro (version 7.5.0.85, Fujitsu Limited, Tokyo, Japan 2006) and GOLD Suite (version 5.2.2, CCDC Software Limited, Cambridge, UK 2013) (flexible ligand/flexible active site residue side chains). Six appropriate docking complexes were selected on the basis of two criteria: a maximum distance of 4 Å between the inhibitors' warhead electrophilic carbon and the CYS277 thiolate; the hydrophobic portion of the inhibitors being satisfactorily buried under the helix 309 – 318 as seen in the crystal structure 2Q3Z.pdb. The complexes were subjected to unrestrained MD in explicit water for 275 ns from which 6 models of TG2 active site were generated. The acrylamide-based inhibitors (**1**–**6**, Table 1) were docked into the resulting active site models. Complexes for these inhibitors were selected using the criteria given above and these were subjected to a further 5 ns of molecular dynamics simulation at 300 K in explicit water.

The complexes that were carried through to the umbrella sampling were either docked complexes from the penultimate stage above (**3**, **4** and **6**) or were snapshots from the final 5 ns MD simulations (**1**, **2** and **5**). For each compound, the structure selected was the one that had the lowest distance between the thiolate sulfur of CYS277 and the compound's electrophilic carbon. Good docking rank and favourable interactions with active site residues (for example, hydrogen bonding with GLN276, ASN333 and PHE334) were also considered in the selection process.

Table 1
Structures and IC_{50} values for the TG2 inhibitors used in this work [15].

Compound	Structure	TG2 IC_{50} (μM)
1	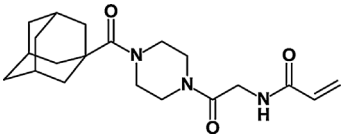	0.125
2	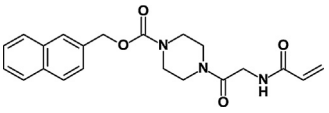	0.44
3	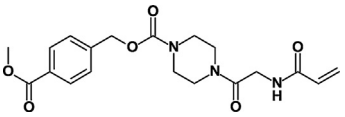	6.3
4	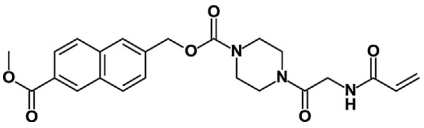	2.1
5	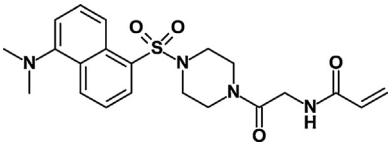	0.0061
6	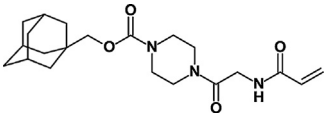	1.625

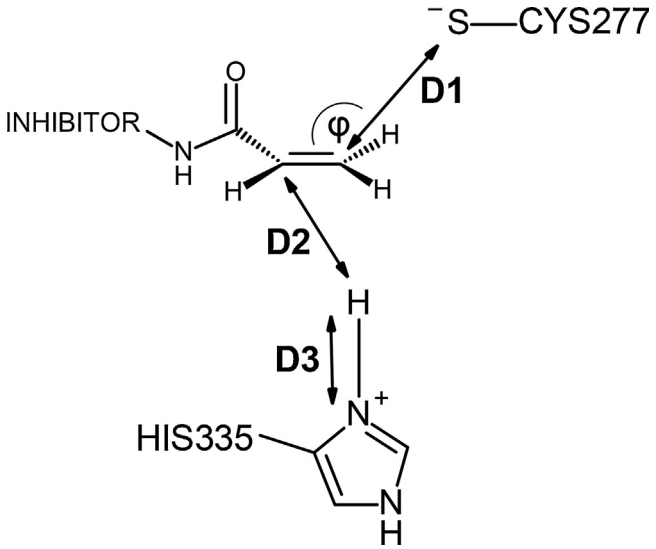

Fig. 2. The distances D1, D2 and D3 together with φ, the angle of approach of the thiolate nucleophile to the acrylamide carbon-carbon double bond.

These complexes were subjected to a further 5 ns molecular dynamics simulation under the same conditions but with the addition of the two distance constraints D1 and D2, outlined in Fig. 2, using a force constant of 500 kcal/mol Å^2 to maintain the initial distances.

This was followed by a 100 ps QM/MM MD equilibration run under constant pressure in TIP3P water. The quantum mechanical (QM) region comprised the ligand, the side chain of CYS277 and the protonated imidazole ring of HIS335. The rest of the system was treated molecular mechanically using the ff99SB force field [32]. In addition, the distances D1 and D2 were restrained to their starting values with a force constant of 50 kcal/mol Å^2.

2.3. Exploration of the reaction coordinate

A study by Paasche et al. [33] indicated that α,β-unsaturated amides, unlike α,β-unsaturated aldehydes, react with thiols preferentially via thiolate attack onto the β-carbon generating a carbanion at the α-position ("direct addition") rather than placing the negative charge on the carbonyl oxygen. The latter scenario would involve a high-energy enolate structure arising from the interruption of the natural tutomeric state of the acrylamide amide group. Instead, the relatively lower-energy carbanion is then protonated by any convenient proton source. Therefore, in order to model the covalent modification of TG2 CYS277 by the inhibitors **1**–**6**, we chose this direct addition pathway rather than the sequence of enolate formation, protonation of the enolate oxygen and finally base-catalysed reformation of the carbonyl group. The protonated imidazole of HIS335, a constituent of the catalytic triad was chosen as the most likely source for the protonation of the initial adducts formed by the attack of CYS277 thiolate upon the acrylamide of each inhibitor. There was no other protein-based proton source near enough to be able to neutralise the negatively charged adducts. For example, the nearest lysine ε-amino group or arginine side-

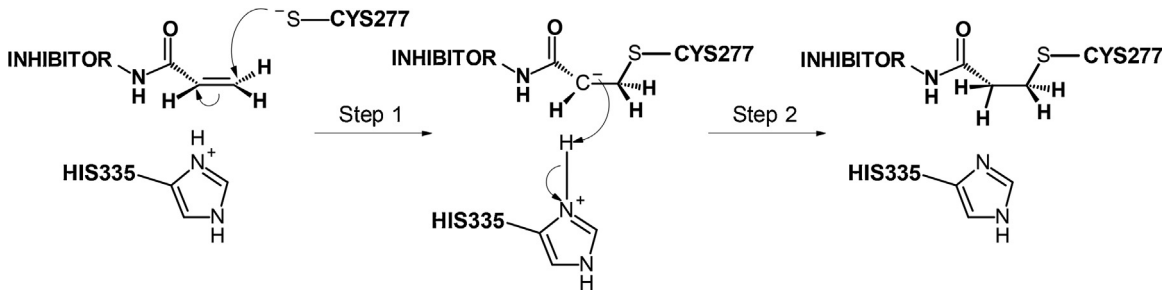

Fig. 3. The approximation of the Michael reaction resulting in covalent modification of CYS277: Step 1–thiolate attack on the β-carbon of the acrylamide; Step 2–proton transfer from HIS335 to the carbanion.

Table 2
Transition state parameters, activation energy (AE), reaction energy (RE) calculated at PM3/AMBERff99SB and the TG2 IC_{50} data for the six acrylamide compounds.

Compound	D1 (Å)	D2 (Å)	RC (Å)	φ (°)	Dihedral (°)	AE (kcal/mol)	RE (kcal/mol)	IC_{50} (μM)
1	1.83	2.06	3.89	98.3	56	42.55	6.66	0.125
2	1.94	1.61	3.54	111.5	72	29.57	8.70	0.44
3	2.15	1.71	3.85	94.5	61	69.71	29.66	6.3
4	1.96	1.91	3.87	114.7	87	40.44	17.57	2.1
5	2.03	1.85	3.89	94.0	80	35.66	−6.70	0.0061
6	1.83	1.63	3.46	110.7	73	63.19	49.69	1.625

chain functionality was at least 9 Å from the required protonation site. Protonation via water molecules within the active site remains a possibility but their number and proximity to the protonation site varied with each inhibitor adduct (and were entirely absent in the simulations involving compounds **2** and **5**) and thus it was not possible to derive a unified approximation to the overall Michael reaction that involved water molecules.

Two approximations of the "direct addition" Michael reaction mechanism for the reaction were explored (Fig. 3). The first involved a single concerted stage only, during which a bond between the nucleophilic sulfur of CYS277 and the β-carbon of the acrylamide was formed and the δ H of the protonated imidazole of HIS335 was transferred to the α-carbon of the acrylamide. The second approximation of the Michael reaction ran these two events consecutively, starting with the thiolate nucleophilic attack.

2.3.1. Umbrella sampling

Each simulation was initiated from the restart file at the end of the 100 ps QM-MM relaxation and two methods were used to calculate the energy of the QM region: PM3 [27] and SCC-DFTB [34,35].

2.3.1.1. Concerted reaction. For the single-stage concerted approximation of the Michael reaction, the reaction coordinate was defined as a generalised distance coordinate involving the sum of distances D1 and D2 (Fig. 2). This reaction coordinate was set to change from its starting value to a value of 2.8 Å (≈1.8 Å for D1 and ≈1 Å for D2). For compound **5** (the most active compound) the same concerted process was also explored using the distances D1 (3.5–1.63 Å) and D2 (5.3–0.9 Å) as separate reaction coordinates and using PM3 as the QM method.

2.3.1.2. Stepwise reaction. For the two-stage approximation of the Michael reaction, the reaction coordinate for the first stage was the single distance D1 (final value 1.6 Å) and the reaction coordinate for the second step was defined as a generalised distance coordinate sampling D2 minus D3 (final value −2 Å). Further details are given in the supplementary information.

2.3.2. Potential of mean force (PMF) calculations

The weighted histogram analysis method (WHAM) [36–38] implemented in the WHAM program [39] was used to calculate the potential of mean force (PMF) from the time profiles for the US simulations. The criteria for successful umbrella sampling simulations were appropriate overlap between the windows of all the simulations, the formation of the relevant new bonds and the fact that the compound maintained its general pose within the TG2 active site at the end of the simulation.

3. Results and discussion

3.1. Single-stage concerted approximation of the Michael reaction

Umbrella sampling simulations involving the generalised distance coordinate (D1 + D2) and SCC-DFTB as the QM method were unable to drive the reaction to completion for compound **2**. In contrast, when PM3 was the applied QM method, all six simulations completed to the assigned value of the reaction coordinate, the two bonds formed, the compounds maintained their original pose within the TG2 active site and a sufficient degree of overlap between the US windows was observed. The PMF values (PM3) were calculated using the WHAM program and plotted against the reaction coordinate for all six compounds (supplementary information, Fig. S**2**). A similar path was followed by all the compounds during their US simulations and the barrier height was reached at a similar value for the reaction coordinate in each case. The time-courses of the relevant angles and atom-atom distances were measured using the VMD program [40]. These are given in the supplementary information, Fig. S**4**. Across the compound set, D1 and D2 declined together. The angle of approach of the attacking thiolate (φ) was observed to be between 94 and 115° at the transition state, straddling the ideal Bürgi–Dunitz angle [41] of 107° for the analogous nucleophilic attack on a carbonyl group. The dihedral angle for the attacking thiolate trajectory was also measured. This is described by the thiolate sulfur, the acrylamide β-carbon, the α-carbon and the carbonyl carbon. At the transition state for the six compounds, values were observed in the range 56–87°. These values, together with φ, indicated an appropriate approach of the thiolate approximately orthogonal to the plane of the acrylamide. After the S-C bond was formed, φ assumed values appropriate for a tetrahedrally-substituted carbon atom. The activation energy (AE) was taken as the difference between the barrier height and the energy of the reactants, the latter being zero in most cases, and the reaction energy (RE) was the energy difference between the

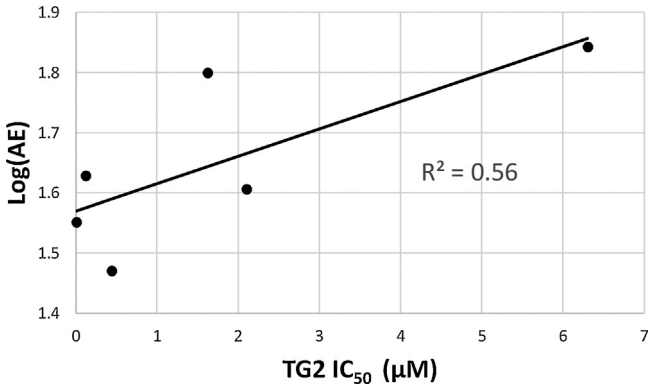

Fig. 4. Plot of activation energy Log(AE) against TG2 IC_{50} for compounds **1** – **6**.

reactants and the products. The values of these parameters for the six inhibitors at the barrier heights are presented in Table 2. For compound **5**, the 2-D free energy surface resulting from umbrella sampling D1 and D2 as separate reaction coordinates gave very similar transition state parameters (distances, angles and charges) to those obtained from the umbrella sampling described above for the generalised distance coordinate D1 + D2, apart from the transition state energy itself. These properties are stated in the supplementary information in **Table S1** together with the corresponding 2-D free energy surface expressed as a contour plot in Fig. S**3**.

The plot of AE against TG2 IC_{50} (Fig. 4) exhibited a trend of increasing AE with decreasing biological activity with $R^2 = 0.56$, rising to 0.79 if the outlier compound **6** is removed. The reaction energies were less realistic in that they indicated that the covalent modification of CYS277 was endothermic in all cases except for the most potent inhibitor, compound **5**. Nevertheless, inspection of the reactions energies was able to rank five out of the six compounds correctly in terms of potency.

Thus the method was able to drive the reaction to completion and to produce activation energies that correlated roughly with the biological activity. However, close inspection of the trajectories revealed a problem with the simulations involving compounds **1**, **3** and **5**. In these cases the starting configurations placed the CYS277 thiolate and the HIS355 π-NH in close proximity. In the early stages of the umbrella sampling the positively-charged imidazole protonated the thiolate. This was confirmed by monitoring the charge on the sulfur atom which had changed from the initial full negative charge to approximately neutral. Under the influence of the imposed reaction coordinate, the resulting CYS277-SH then moved onto the inhibitor acrylamide alkene and completed the carbon-sulfur bond formation and the proton transfer to carbon essentially simultaneously. In contrast, for compounds **2**, **4** and **6**, the CYS277 thiolate and the HIS355 π-NH were not in close proximity in the starting configurations. In the course of the umbrella sampling the CYS277 thiolate retained its full negative charge until the moment of sulfur-carbon bond formation. There followed a period where the former acrylamide α-carbon and the carbonyl oxygen shared approximately one whole negative charge between them. This is consistent with the expected delocalisation of the charge across these atoms. Finally, the proton was transferred from the positively-charged HIS355 to the α-carbon of the former acrylamide of the inhibitor.

This lack of uniformity across the six inhibitors was the spur to simulate the Michael reaction in a discrete two-stage process.

3.2. Consecutive two-stage approximation of the Michael reaction

Both SCC-DFTB and PM3-based calculations were successful in driving both stages of the Michael reaction to completion and resulted in plausible structures and no change in the final position of the inhibitor. As in the case of the single-stage concerted version of the Michael reaction, the activation energy (AE) was taken as the difference between the barrier height and the energy of the reactants. For the PM3-based calculations, however, no meaningful correlation could be made between biological activity and the calculated activation energy. In contrast, SCC-DFTB-based calculations yielded useful correlations. Therefore, only the results for SCC-DFTB will be presented. A relatively high value of 250 kcal/mol $Å^2$ for the force constant was necessary to drive the reactions to completion. This is consistent with the work published by Silva et al. [42] who used the same force constant whilst investigating the inhibition of mycobacterial L,D-transpeptidase 2 by carbapenems. In that case the process involved a similar nucleophilic attack of an active site cysteine thiolate upon the carbonyl carbon atom of a carbapenem. A proton was transferred in the second step from a nearby histidine residue to saturate the resulting amino nitrogen.

3.2.1. First stage: attack of the thiolate anion

At the end of this simulation stage, the new S-C bond was present for all the inhibitors and the final conformations were used as the starting points for the second stage. The calculated PMF plots are shown in Fig. 5. In each case a saddle was observed in the region of RC = 2 Å. This was selected to be the TS corresponding to the first stage.

For the six inhibitors, the structures at the saddle points had very similar values for D1 and φ and the values of φ and the dihedral angle indicated an appropriate approach of the thiolate approximately orthogonal to the plane of the acrylamide. Along the reaction coordinate, the charge on the CYS277 thiolate was observed to change from the initial full negative charge to a value around −0.5 at the saddle point. These transition state parameters are summarised in Table 3 along with the PMF activation ener-

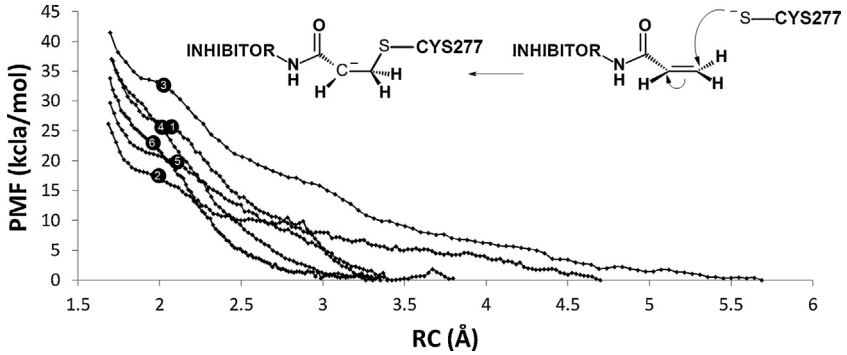

Fig. 5. Plots of PMF against RC for compounds **1**–**6** during the first step (attack of the thiolate anion to give a carbanion-containing product as shown). The markers (containing the compound number) represent the TS position. The reaction proceeds from higher to lower RC values.

Table 3
Transition state parameters for first stage (thioate attack; calculated at SCC-DFTB/AMBERff99SB) of the two-stage approximation of the Michael reaction.

Compound	D1 (Å)	φ (°)	Dihedral (°)	Charge S	AE (kcal/mol)
1	2.08	114	84	−0.49	25.67
2	1.99	114	64	−0.40	17.45
3	2.03	114	57	−0.55	32.61
4	2.01	124	80	−0.59	25.61
5	2.11	120	63	−0.53	19.68
6	1.96	113	76	−0.48	22.95

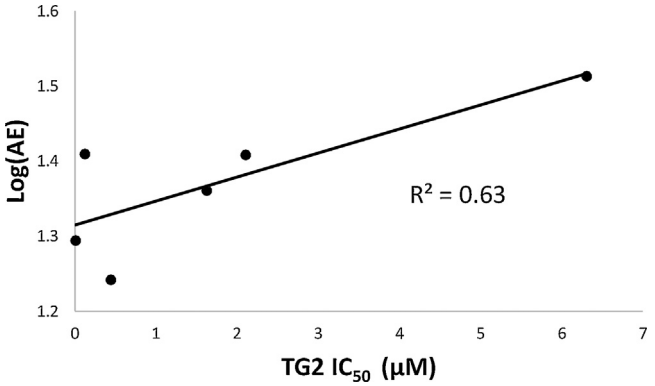

Fig. 6. Plot of Log(AE) against TG2 IC_{50} for the 1st stage (thiolate attack) of the 2-stage simulations for acrylamide compounds **1** – **6**.

gies at that point for each compound. The latter showed reasonable correlation with TG2 IC_{50} with an R^2 of 0.63 (Fig. 6).

3.2.2. Second stage: proton transfer from HIS335 to the α-carbon of the former acrylamide

The method was able to drive this stage to completion and the protonation of the α-carbon was evident for all the compounds. The overlap between the US windows achieved was reasonable although the windows were apparent in the WHAM-generated PMF plots in the shape of curves corresponding to each window (Fig. 7). For each compound, the highest point on the curve in the RC range 2–0 was taken to be the transition state or the barrier height for the second stage. It is represented in Fig. 7 by markers containing the compound numbers.

The TS structures occurred over RC values 0.4–1.1 Å. In all cases, at the TS, HIS335 remained protonated. The charges on the acrylamide carbonyl oxygen and the α-carbon indicated that the negative charge was delocalised over these atoms. The activation energy for the 2nd stage (protonation) correlated well with biological activity with an R^2 of 0.80 (Fig. 8). The TS parameters are given in Table 4.

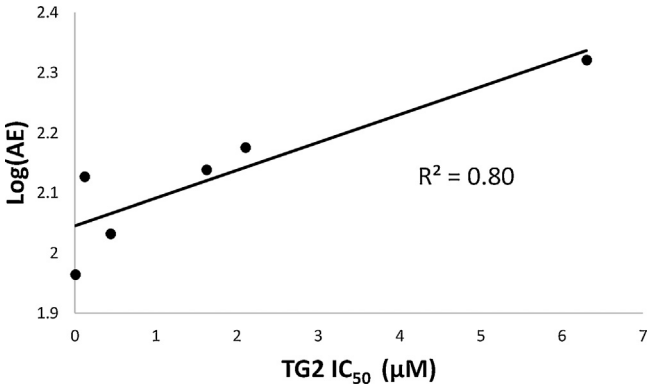

Fig. 8. Plot of Log(AE) against TG2 IC_{50} for the 2nd stage (protonation) of the 2-stage simulations for acrylamide compounds **1** – **6**.

Table 4
Transition state parameters for the second stage (protonation; calculated at SCC-DFTB/AMBERff99SB) of the two-stage approximation of the Michael reaction using DFTB as the QM method.

Comp.	RC (Å)	D2 (Å)	D3 (Å)	Charge O	Charge α-C	AE (kcal/mol)
1	0.85	1.94	1.10	−0.72	−0.60	134.27
2	0.70	1.80	1.09	−0.57	−0.57	107.95
3	0.85	1.91	1.11	−0.70	−0.56	209.74
4	0.34	1.48	1.09	−0.62	−0.56	150.15
5	1.13	2.19	1.06	−0.65	−0.61	92.24
6	0.48	1.63	1.03	−0.67	−0.56	137.73

3.2.3. Charge time profile across the two stages of simulation and the relative activation energies

As can be seen from Fig. 9 the time courses of charge variation on the key atoms in the reaction centre (CYS277 sulfur, the acrylamide carbonyl oxygen and α-carbon) were similar across all six compounds when viewed for steps one and two combined. In each case as the first stage progressed, the charges on the α-carbon and the carbonyl oxygen became more negative, reaching their most negative by the end of the first stage. Simultaneously, the full negative charge on the cysteine sulfur moderated to approximately −0.3. This is consistent with the negative charge being passed from the sulfur to be delocalised across the α-carbon and the carbonyl oxygen. The activation energy values for the first stage (the formation of the sulfur-carbon bond) were lower than those for the second stage (the protonation step) suggesting that the latter is the rate limiting step for this reaction. This is in contrast to the traditional view for a small-molecule thiol Michael addition reaction where the attack of the thiolate is considered to be the rate limiting step [43]. In the present case with the simulation of the TG2 inhibitory action of compounds **1**–**6**, it happens that the approach of the acrylamide warhead to the CYS277 thiolate is energetically easier than the distortion of the protein necessary to allow HIS355 to

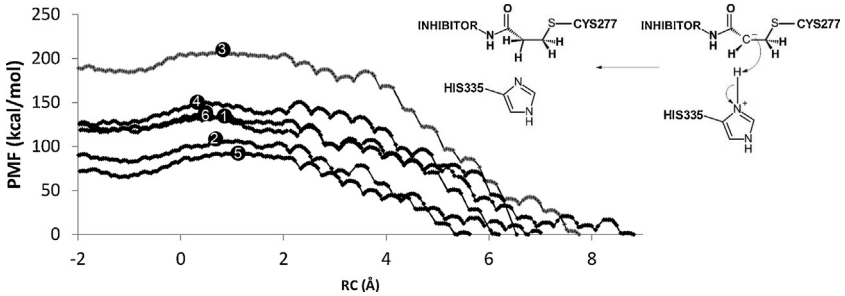

Fig. 7. PMF graphs of the 6 compounds for the 2nd stage of the 2-stage US simulations using DFTB as the QM method. The markers (containing the compound number) represent the TS position. The reaction proceeds from higher to lower RC values.

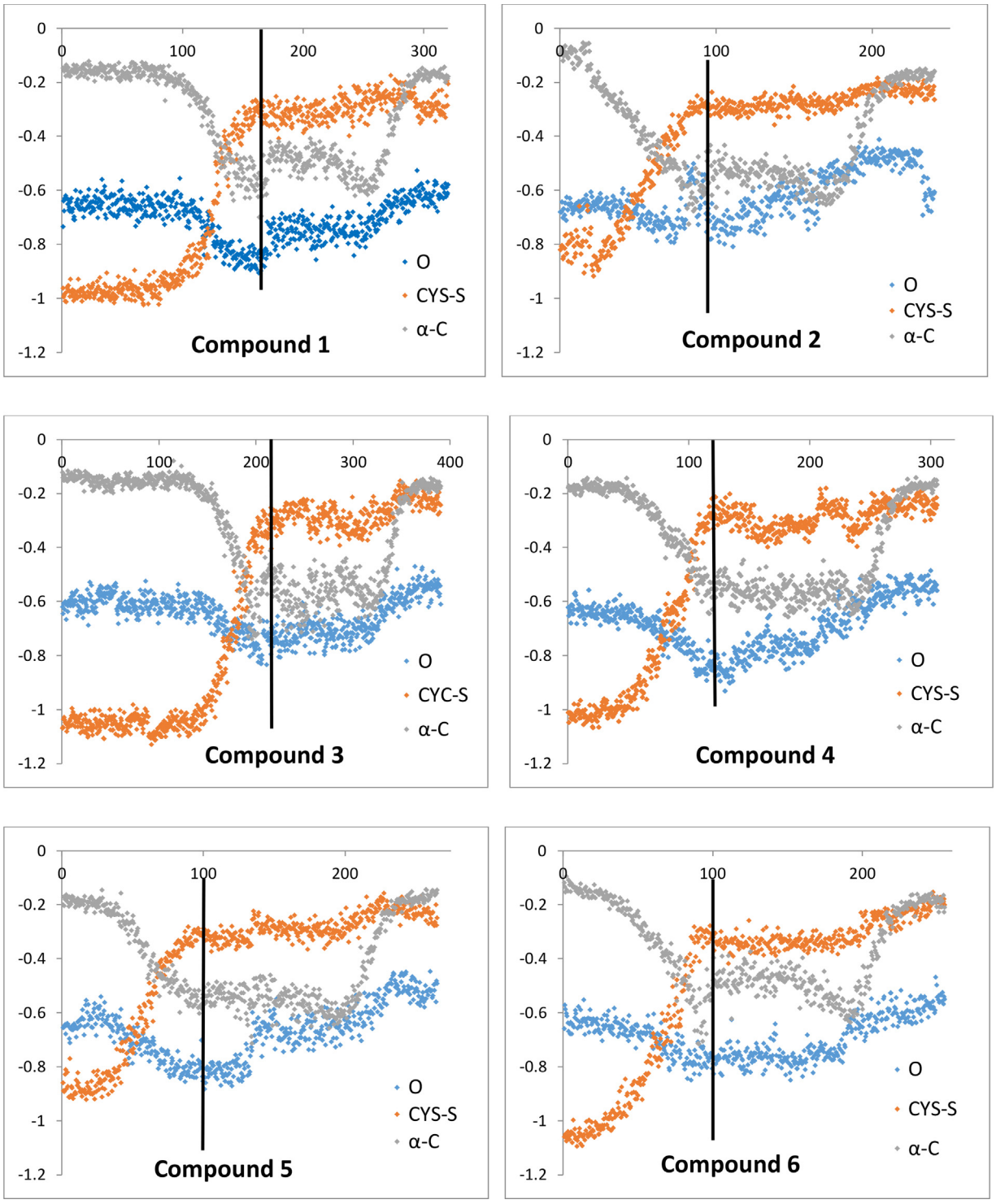

Fig. 9. The time courses of the charges on the CYS277 sulfur, the acrylamide carbonyl oxygen and α-carbon. The X-axis has the simulation time in ps and the Y-axis records the charge. The vertical line marks the end of the 1st step.

perform the second stage protonation. An alternative proton source may have been better in this regard, but, as mentioned earlier, the only other possibility would be a water molecule and for two of the simulations (compounds **2** and **5**) there were no water molecules present in the active site.

3.2.4. Distance time profile across the two stages of simulation

The time profile of the key atom-atom distances (D1, D2 and D3) followed very similar patterns across the compound set and were under the control of the reaction coordinates of the two stages at all times. This is exemplified in Fig. 10 for compound **6** where the distance time course is given for both stages of simulation.

4. Conclusion

Good or reasonable correlations were observed between the TG2 IC_{50} data and the activation energies for first stage (thiolate attack; R^2 0.63), the second stage (protonation; R^2

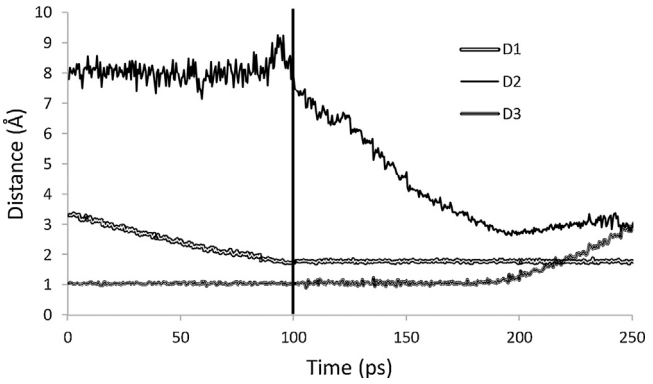

Fig. 10. Key atom-atom distance time course for the simulation of compound 6. The vertical line marks the end of the first stage.

0.89) but less so for the single-stage approach (combined thiolate attack and protonation; R^2 0.56). In light of this it appears that under the conditions of the assay [44], the covalent modification of the active site cysteine is rate-limiting compared with the generation of the initial protein-inhibitor complex. In each of the six piperazinylglycylacrylamide-based TG2 inhibitors considered in this study, the point of variation was the hydrophobic aryl/adamantly substituent with its associated amide/carbamate/sulphonamide link to the piperazine core. The effect of these substituents in the protein-ligand docking experiments and subsequent molecular dynamics simulations was to anchor the inhibitors slightly differently in the TG2 active site particularly with respect to the exact location of the acrylamide warhead relative to the CYS277 thiolate. That in turn gave rise to the differences in the activation energies observed for the imposed reaction coordinates. Furthermore, the positioning of the warhead in the active site tunnel did not allow the presence of active-site water molecules for the simulations involving compounds **2** or **5** and for the other compounds interaction with water was limited, there being respectively 1, 1, 2 and 1 water molecules making hydrogen bonding contact with the CYS277 thiolate anion for the simulations involving compounds **1**, **3**, **4** and **6.** It is therefore highly unlikely that desolvation of the thiolate anion is a major concern on the reaction pathway for the inhibitory action of these compounds. This is in contrast to the work of Capoferri et al. [45], who studied the Michael-type direct addition of an acrylamide-based inhibitor to the solvent-accessible CYS797 of epidermal growth factor receptor at the SCC-DFTB/AMBER99SB level. In that case desolvation of the thiolate anion was the key step of the overall process rather than the carbon-sulfur bond formation and subsequent protonation of the transient carbanion.

Overall, this approximation of the thiolate Michael reaction is a reasonable approach for the evaluation of acrylamide-based potential TG2 inhibitors *in silico*: Protein-ligand docking combined with molecular dynamics and biochemically-relevant selection criteria were observed to be enough to weed out the non-potent compounds. Thereafter, the QM/MM MD umbrella sampling approaches described above were able to provide a reasonable correlation between activation energies and TG2 IC_{50} over the range 0.0061–6.3 μM (three orders of magnitude) for use with compound ranking.

Appendix A. Supplementary data

Supplementary data associated with this article can be found, in the online version, at https://doi.org/10.1016/j.jmgm.2017.10.012.

References

[1] M. Griffin, R. Casadio, C.M. Bergamini, Transglutaminases: nature's biological glues, Biochem. J. 368 (2002) 377–396, http://dx.doi.org/10.1042/BJ20021234.
[2] E. Badarau, R.J. Collighan, M. Griffin, Recent advances in the development of tissue transglutaminase (TG2) inhibitors, Amino Acids 44 (2013) 119–127, http://dx.doi.org/10.1007/s00726-011-1188-4.
[3] M. Siegel, C. Khosla, Transglutaminase 2 inhibitors and their therapeutic role in disease states, Pharmacol. Ther. 115 (2007) 232–245, http://dx.doi.org/10.1016/j.pharmthera.2007.05.003.
[4] B. Min, Y.-C. Kwon, K.-M. Choe, K.C. Chung, PINK1 phosphorylates transglutaminase 2 and blocks its proteasomal degradation, J. Neurosci. Res. 93 (2015) 722–735, http://dx.doi.org/10.1002/jnr.23535.
[5] S. Altuntas, M. D'Eletto, F. Rossin, et al., Type 2 Transglutaminase, mitochondria and Huntington's disease: Menage a trois, Mitochondrion 19 (2014) 97–104, http://dx.doi.org/10.1016/j.mito.2014.09.008.
[6] H. Grosso, M.M. Mouradian, Transglutaminase 2: biology, relevance to neurodegenerative diseases and therapeutic implications, Pharmacol. Ther. 133 (2012) 392–410, http://dx.doi.org/10.1016/j.pharmthera.2011.12.003.
[7] C. Klöck, T.R. DiRaimondo, C. Khosla, Role of transglutaminase 2 in celiac disease pathogenesis, Semin. Immunopathol. 34 (2012) 513–522, http://dx.doi.org/10.1007/s00281-012-0305-0.
[8] M.K. Park, H.J. Lee, J. Shin, et al., Novel participation of transglutaminase-2 through c-Jun N-terminal kinase activation in sphingosylphosphorylcholine-induced keratin reorganization of PANC-1 cells, Biochim. Biophys. Acta 1811 (2011) 1021–1029, http://dx.doi.org/10.1016/j.bbalip.2011.07.007.
[9] M.K. Park, H.J. You, H.J. Lee, et al., Transglutaminase-2 induces N-cadherin expression in TGF-β1-induced epithelial mesenchymal transition via c-Jun-N-terminal kinase activation by protein phosphatase 2A down-regulation, Eur. J. Cancer 49 (2013) 1692–1705, http://dx.doi.org/10.1016/j.ejca.2012.11.036.
[10] T.M. Jeitner, E.J. Delikatny, J. Ahlqvist, et al., Mechanism for the inhibition of transglutaminase 2 by cystamine, Biochem. Pharmacol. 69 (2005) 961–970, http://dx.doi.org/10.1016/j.bcp.2004.12.011.
[11] C. Pardin, J.N. Pelletier, W.D. Lubell, et al., Cinnamoyl inhibitors of tissue transglutaminase, J. Org. Chem. 73 (2008) 5766–5775, http://dx.doi.org/10.1021/jo8004843.
[12] N.S. Caron, L.N. Munsie, W.D. Keillor, et al., Using FLIM-FRET to measure conformational changes of transglutaminase type 2 in live cells, PLoS One 7 (2012) e44159, http://dx.doi.org/10.1371/journal.pone.0044159.
[13] A. Case A, R.L. Stein, Kinetic analysis of the interaction of tissue transglutaminase with a nonpeptidic slow-binding inhibitor, Biochemistry 46 (2007) 1106–1115, http://dx.doi.org/10.1021/bi061787u.
[14] Z. Wang, M. Griffin, TG2, a novel extracellular protein with multiple functions, Amino Acids 42 (2012) 939–949, http://dx.doi.org/10.1007/s00726-011-1008-x.
[15] E. Badarau, Z. Wang, D.L. Rathbone, et al., Development of potent and selective tissue transglutaminase inhibitors: their effect on TG2 function and application in pathological conditions, Chem. Biol. 22 (2015) 1347–1361, http://dx.doi.org/10.1016/j.chembiol.2015.08.013.
[16] E. Badarau, A. Mongeot, R. Collighan, et al., Imidazolium-based warheads strongly influence activity of water-soluble peptidic transglutaminase inhibitors, Eur. J. Med. Chem. 66 (2013) 526–530, http://dx.doi.org/10.1016/j.ejmech.2013.05.018.
[17] M. Griffin, A. Mongeot, R. Collighan, et al., Synthesis of potent water-soluble tissue transglutaminase inhibitors, Bioorg. Med. Chem. Lett. 18 (2008) 5559–5562, http://dx.doi.org/10.1016/j.bmcl.2008.09.006.
[18] D. Halim, K. Caron K, J.W. Keillor, Synthesis and evaluation of peptidic maleimides as transglutaminase inhibitors, Bioorg. Med. Chem. Lett. 17 (2007) 305–308, http://dx.doi.org/10.1016/j.bmcl.2006.10.061.
[19] C. Pardin, S.M.F.G. Gillet, J.W. Keillor, Synthesis and evaluation of peptidic irreversible inhibitors of tissue transglutaminase, Bioorg. Med. Chem. 14 (2006) 8379–8385, http://dx.doi.org/10.1016/j.bmc.2006.09.011.
[20] C. Marrano, P. De Macédo, J.W. Keillor, Evaluation of novel dipeptide-bound é,α-unsaturated amides and epoxides as irreversible inhibitors of guinea pig liver transglutaminase, Bioorg. Med. Chem. 9 (2001) 1923–1928, http://dx.doi.org/10.1016/S0968-0896(01)00101-8.
[21] M. Griffin, D. Rathbone, L. Badarau, Acylpiperazines as Inhibitors of Transglutaminase and Their Use in Medicine, 2017 (International Publication Number WO 2014/057266 Al).
[22] D.A. Case, T.A. Darden, T.E. Cheatham III, et al., University of California, 12, AMBER, San Francisco, 2012.
[23] R. Salomon-Ferrer, A.W. Goetz, D. Poole, et al., Routine microsecond molecular dynamics simulations with AMBER – Part II: particle Mesh Ewald, J. Chem. Theory Comput. 9 (2013) 3878–3888, http://dx.doi.org/10.1021/ct400314y.
[24] A.W. Goetz, M.J. Williamson, D. Xu, et al., Routine microsecond molecular dynamics simulations with AMBER – Part I: Generalized Born, J. Chem. Theory Comput. 8 (2012) 1542–1555, http://dx.doi.org/10.1021/ct200909j.
[25] S. Le Grand, A.W. Goetz, R.C. Walker, SPFP: speed without compromise – a mixed precision model for GPU accelerated molecular dynamics simulations, Comp. Phys. Comm. 184 (2013) 374–380, http://dx.doi.org/10.1016/j.cpc.2012.09.022.

[26] R.C. Walker, M.F. Crowley, D.A. Case, The implementation of a fast and accurate QM/MM potential method in Amber, J. Comput. Chem. 29 (2008) 1019–1031, http://dx.doi.org/10.1002/jcc.20857.
[27] J.J.P. Stewart, Optimization of parameters for semiempirical methods I. Method, J. Comput. Chem. 10 (1989) 209–220, http://dx.doi.org/10.1002/jcc.540100208.
[28] D.R. Roe, T.E. Cheatham III, PTRAJ and CPPTRAJ: software for processing and analysis of molecular dynamics trajectory data, J. Chem. Theory Comput. 9 (2013) 3084–3095, http://dx.doi.org/10.1021/ct400341p.
[29] D.M. Pinkas, P. Strop, A.T. Brunger, et al., Transglutaminase 2 undergoes a large conformational change upon activation, PLoS Biol. 5 (2007) 2788–2796, http://dx.doi.org/10.1371/journal.pbio.0050327.
[30] J.W. Keillor, C.M. Clouthier, K.Y.P. Apperley, et al., Apperley, et al, Acyl transfer mechanisms of tissue transglutaminase, Bioorg. Chem. 57 (2014) 186–197, http://dx.doi.org/10.1371/10.1016/j.bioorg.2014.06.003.
[31] S.E. Iismaa, S. Holman, M. Wouters, et al., Evolutionary specialization of a tryptophan indole group for transition-state stabilization by eukaryotic transglutaminases, PNAS 100 (2003), http://dx.doi.org/10.1073/pnas.1635052100.
[32] V. Hornak, R. Abel, A. Okur, et al., Comparison of multiple Amber force fields and development of improved protein backbone parameters, Proteins 65 (2006) 712–725, http://dx.doi.org/10.1002/prot.21123.
[33] A. Paasche, M. Schiller, T. Schirmeister, B. Engels, Mechanistic study of the reaction of thiol-Containing enzymes with α,β-Unsaturated carbonyl substrates by computation and chemoassays, Chem. Med. Chem. 5 (2010) 869–880, http://dx.doi.org/10.1002/cmdc.201000020.
[34] M. Elstner, D. Porezag, G. Jungnickel, et al., Self-consistent-charge density-functional tight-binding method for simulations of complex materials properties, Phys. Rev. B 58 (1998) 7260–7268, http://dx.doi.org/10.1103/PhysRevB.58.7260.
[35] G. de M. Seabraa, R.C. Walker, M. Elstner M, et al., Implementation of the SCC-DFTB Method for Hybrid QM/MM Simulations within the Amber Molecular Dynamics Package, J. Phys. Chem. A 111 (2007) 5655–5664, http://dx.doi.org/10.1021/jp070071l.
[36] M. Souaille, B. Roux, Extension to the weighted histogram analysis method: combining umbrella sampling with free energy calculations, Comput. Phys. Commun. 135 (2001) 40–57, http://dx.doi.org/10.1016/S0010-4655(00)00215-0.
[37] J.S. Hub, B.L. De Groot, D. Van Der Spoel, g-wham-A free Weighted Histogram Analysis implementation including robust error and autocorrelation estimates, J. Chem. Theory Comput. 6 (2010) 3713–3720, http://dx.doi.org/10.1021/ct100494z.
[38] S. Kumar, J.M. Rosenberg, D. Bouzida, et al., Multidimensional free-energy calculations using the weighted histogram analysis method, J. Comput. Chem. 16 (1995) 1339–1350, http://dx.doi.org/10.1002/jcc.540161104.
[39] A. Grossfield, WHAM: the Weighted Histogram Analysis Method, 2013 http://membrane.urmc.rochester.edu/content/wham.
[40] W. Humphrey, A. Dalke, K. Schulten, VMD: visual molecular dynamics, J. Mol. Graph. 14 (1996) 33–38, http://dx.doi.org/10.1016/0263-7855(96)00018-5.
[41] H.B. Bürgi, J.D. Dunitz, J.M. Lehn, et al., Stereochemistry of reaction paths at carbonyl centres, Tetrahedron 30 (1974) 1563–1572, http://dx.doi.org/10.1016/S0040-4020(01)90678-7.
[42] J.R.A. Silva, T. Govender, G.E.M. Maguire, et al., Simulating the inhibition reaction of *Mycobacterium tuberculosis* L,D-transpeptidase 2 by carbapenems, Chem. Commun. 51 (2015) 12560–12562, http://dx.doi.org/10.1039/C5CC03202D.
[43] D.P. Nair, M. Podgorski, S. Chatani, et al., The thiol-Michael addition click reaction: a powerful and widely used tool in materials chemistry, Chem. Mater. 26 (2014) 724–744, http://dx.doi.org/10.1021/cm402180t.
[44] Z. Wang, R.J. Collighan, K. Pytel, D.L. Rathbone, X. Li, M. Griffin, Characterization of heparin-binding site of tissue transglutaminase its importance in cell surface targeting, matrix deposition, and cell signaling, J. Biol. Chem. 287 (2012) 13063–13083, http://dx.doi.org/10.1074/jbc.M111.294819.
[45] L. Capoferri, A. Lodola, S. Rivara, M. Mor, Quantum Mechanics/Molecular mechanics modeling of covalent addition between EGFR-Cysteine 797 and N-(4-Anilinoquinazolin-6yl) acrylamide, J. Chem. Inf. Model. 55 (2015) 589–599, http://dx.doi.org/10.1021/ci500720e.